Acceleration of a Diels–Alder reaction by a self-assembled molecular capsule

Jongmin Kang & Julius Rebek Jr

Department of Chemistry, Massachusetts Institute of Technology, Cambridge, Massachusetts 02139, USA and The Skaggs Institute for Chemical Biology, The Scripps Research Institute, 10550 North Torrey Pines Road, La Jolla, California 92037, USA

THE interior of cage-like molecules can be considered to provide a new phase of matter[1,2], in which it becomes possible to stabilize reactive intermediates[3] and to observe new forms of stereoisomerism[4]. Cage-like molecular complexes that self-assemble through weak intermolecular forces are dynamic species[5,6], encapsulating guest molecules reversibly. They can persist over timescales ranging from microseconds to hours, long enough for chemical processes to take place within them. Here we report the acceleration of a Diels–Alder reaction by encapsulation of the reactants in a self-assembling molecular capsule[7,8]. Although product inhibition (lack of dissociation) prevents the system from showing true catalytic behaviour, there is clear evidence for a rate increase of over two orders of magnitude owing to the effective enhancement of concentration inside the capsule.

Compound **1** (Fig. 1) and its congeners self-assemble in organic solvents to form dimeric capsules[7,8]. The molecules feature self-complementary patterns of hydrogen-bonding sites and a dimer is formed when the concave surfaces of two molecules come together (Fig. 1). Intermolecular hydrogen bonds hold the two subunits together in much the same manner that the stitches along the seam hold a softball together. In aromatic solvents such as benzene, the dimerization constant is large ($>10^6\,M^{-1}$) and the dynamics of assembly are slow on the NMR timescale but fast on the human timescale (< seconds). The dimers can encapsulate molecules of complementary size and shape and do so reversibly. Adamantanes, ferrocene derivatives and [2,2] paracyclophane are among the sizeable guests that fit well within these capsules. The demonstration that two molecules of solvent benzene are accommodated inside[8], raised the possibility of the use of these capsules as chambers for bimolecular reactions.

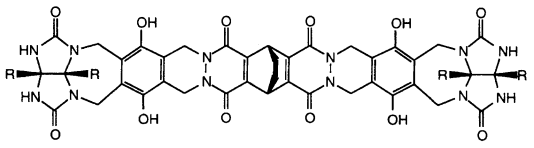

1 R = 4-*n*-heptylphenyl

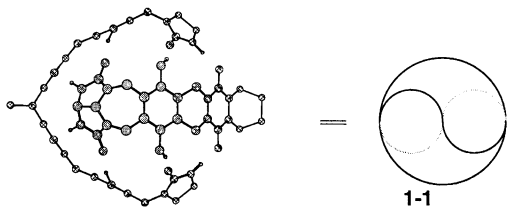

FIG. 1 Representations of the monomeric **1** and its self-assembling dimeric form **1-1**. The hydrogen-bonding network of the dimeric form as an energy-minimized structure generated by MacroModel[22] is highlighted in the cross-section on the left; other atoms have been deleted for viewing clarity. The 'softball' representation is on the right.

With this in mind, we investigated the Diels–Alder reaction between *p*-quinone **2** and cyclohexadiene **3**:

(1)

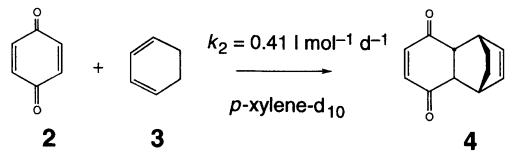

The reaction is slow at room temperature. In *p*-xylene-d_{10} at molar concentrations of each component, the half-life is about two days ($k_2 = 0.41\,l\,mol^{-1}\,d^{-1}$); at millimolar concentrations no product is detected by NMR in a week, as the corresponding half-life is of the order of a year. The stereochemistry of the product **4** is that anticipated for the usual *endo* orientation of reactants in the transition state.

In dilute solution (for example, 1 mM) the Diels–Alder adduct **4** is readily encapsulated by the dimeric **1-1**:

(2)

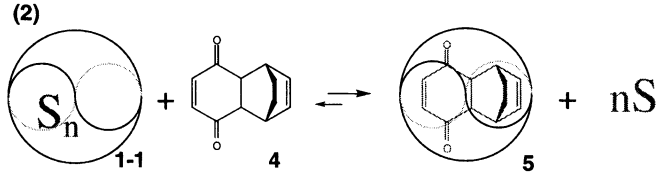

S = *p*-xylene-d_{10}

and NMR signals unique to the encapsulated species **5** can be observed. The widely separated and relatively sharp signals for the free and bound forms of **4** indicate slow exchange of the guest into and out of the host capsule on the NMR timescale (Fig. 2*a–c*). The adduct is a welcome guest; the binding affinity is too large for accurate determination through NMR titrations, and only a lower limit, $K_a > 10^5\,M^{-1}$ can be placed on the association constant. This figure leaves little doubt that the cavity is roomy enough to accommodate the transition-state geometry of this Diels–Alder reaction.

With both *p*-quinone and cyclohexadiene (4 mM each) are added to a solution of the dimeric capsule (1 mM) in *p*-xylene-d_{10} at room temperature, a new, well defined complex emerges, as evidenced by the NMR spectrum (Fig. 3*a*, *b*). One species dominates in the spectrum and a signal for encapsulated quinone is observed. No signals unique to encapsulated cyclohexadiene can be assigned, but some must be present inside because the signals for the encapsulated adduct appear within one day. These signals continue to grow at the expense of the signal for encapsulated quinone (Fig. 3*c*, *d*).

The probably precursor to **5** (complex **6**, reaction (3)) can be regarded as the counterpart of a Michaelis complex, as it converts to product in a first-order process. Consistent with this treatment, observed rates at various cyclohexadiene concentrations (1–7 mM) show saturation kinetics; the parameters at ambient temperature are $V_{max} = 0.001\,M^{-1}\,d^{-1}$ and $k_{cat} = 1\,d^{-1}$ (Fig. 4). The implication is that the Diels–Alder reaction takes place inside the capsule:

(3)

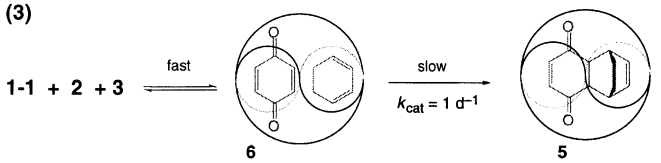

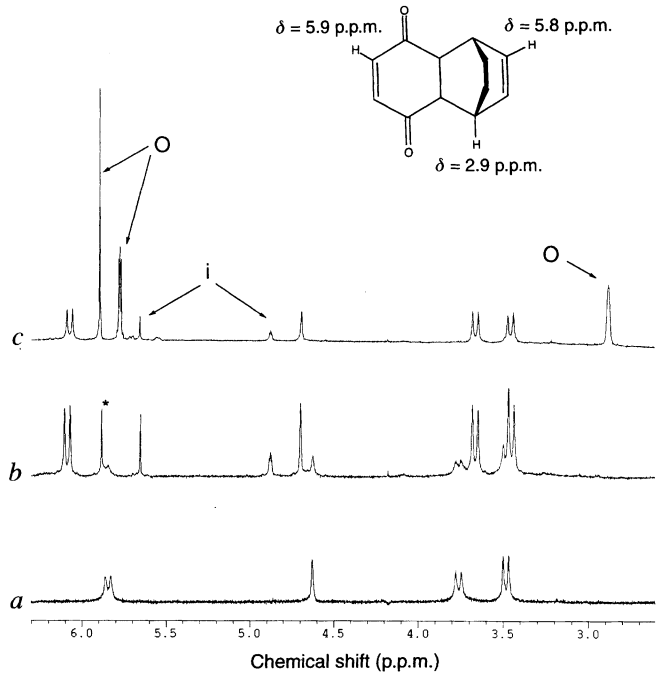

FIG. 2 Proton NMR spectra of **1-1** and its encapsulation complex with the adduct **4** in *p*-xylene-d_{10}. Signals of the guest inside the capsule and outside (free) are labelled with 'i' and 'o', respectively. The signal designated with an asterisk represents chloroform. *a*, Compound **1-1** alone. *b*, Compound **1-1** with 0.7 equiv. of Diels–Alder adduct **4** added; all of the latter is encapsulated and separate signals are observed for the complex **5** and solvated dimer **1-1**. *c*, Compound **1-1** with 6 equiv. of Diels–Alder adduct **4** added; all of the capsule is occupied as complex **5** and separate signals are observed for free and encapsulated adduct **4**. Assignments for resonances of free **4** are shown on the structure.

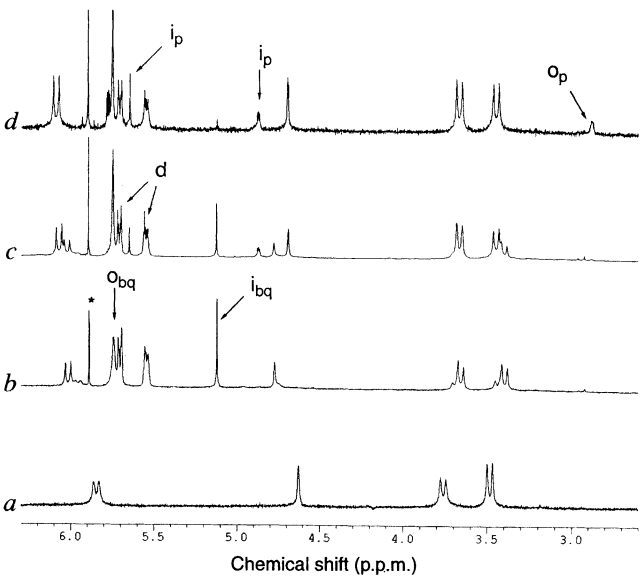

FIG. 3 Changes in the proton NMR spectra of **1-1** during the reaction of *p*-benzoquinone **2** and 1,3-cyclohexadiene **3** in *p*-xylene-d_{10}. The signals for *p*-benzoquinone(bq) and Diels–Alder product (p) inside and outside are designated as 'i' and 'o' respectively. Signals from cyclohexadiene are designated as 'd'. The signal designated with an asterisk represents chloroform impurity. *a*, Compound **1-1** alone. *b*, Shortly after 4 equiv. of *p*-benzoquinone and 4 equiv. of 1,3-cyclohexadiene were added to the solution of **1-1**. *c*, The reaction mixture after 2 days. *d*, The reaction mixture after 19 days, showing evidence of released product and **5** as the principal species.

After several days at ambient temperature some of the adduct appears outside the capsule (Fig. 3*d*), but it is clear that product inhibition is a serious problem and prevents the system from turning over and being an effective catalyst. Indeed, addition of adduct **4** or other good guests (benzene, [2,2] paracyclophane) effectively inhibit the reaction. Nonetheless, the effect of the dimer **1-1** on the reaction rate is impressive; the reaction is accelerated some 200-fold under these conditions.

Are the rate accelerations provided by **1-1** for the Diels–Alder reaction due to encapsulation of the components, or some more conventional form of catalysis? For example, the Diels–Alder reaction is known to be catalyzed by biphenylenediols[9] that can form hydrogen bonds with the carbonyl oxygens of suitable dienophiles. Many hydrogen-bonding sites are featured on the periphery of **1**, but two control experiments to test this possibility with **9** and **10** (Fig. 5) argue against this form of catalysis. The first involved a molecule that bears the same functionalities as **1** but differs in shape, while the second involved a molecule that bears the same shape as **1** but differs in functionalities. Neither **9** nor **10**

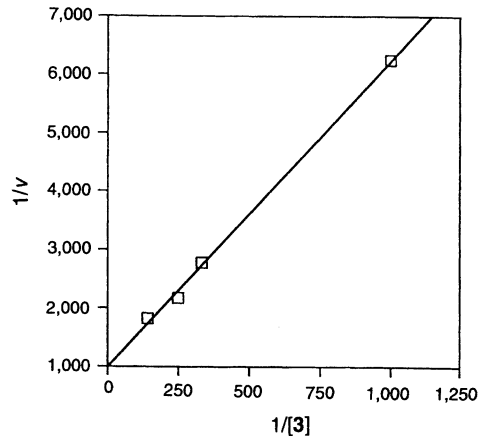

FIG. 4 Lineweaver–Burke plot of the reaction rates, *V*, of **2** with **3** in the presence of **1-1**. The concentrations of 1,3-cyclohexadiene **3** were changed with a constant concentration (4 mM) of *p*-benzoquinone.

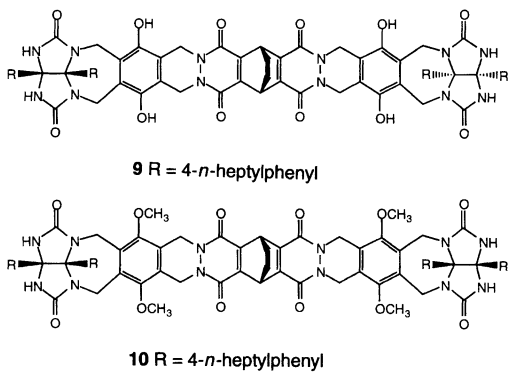

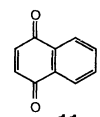

FIG. 5 Compounds used as controls. The reaction of **2** with **3** was not accelerated by the S-shaped stereoisomer **9** in which the glycoluril substituents are on opposite faces of the structure. Nor was it accelerated by the C-shaped structure **10** in which the phenolic units are methylated and the glycoluril substituents are on the same face of the structure. The dimeric form **1-1** did not effect the rate of the Diels–Alder reactions between naphthoquinone **11** and **3**.

accelerated the reaction. Accordingly, acid catalysis through hydrogen bonding to the phenols or the glycoluril functions can be excluded as the source of acceleration. Although some form of acid catalysis might operate within the special microenvironment presented by the capsule to guests, this possibility remains untested, and may even be untestable. Finally, the corresponding reaction of 1,4 naphthoquinone **11**, a molecule too large for the capsule, was not accelerated by **1-1**. The factors of size selectivity, saturation kinetics, and product inhibition all support an encapsulated transition state.

The transition-state geometry of this reaction leading to the *endo* product is reminiscent, in size and shape, of two encapsulated benzene molecules oriented in a face-to-face stacking interaction. Accordingly, the acceleration of the Diels–Alder reaction inside the capsule is not unreasonable. Acceleration of the reverse of the Diels–Alder reaction by encapsulation is unreasonable, and we interpret the accelerating effect of encapsulation on the forward rate as resulting from an enhanced concentration of the reactants inside the capsule, rather than some special stabiization of the transition state. Using a technique described elsewhere[10], we estimate the interior volume of the capsule to be ~300 Å^3. When this space is occupied with one molecule of quinone and cyclohexadiene, the concentration of each reactant inside the capsule is calculated to be about 5 M—this is 1,000 times the concentration of the reactants in the bulk solution (4 mM). Consistent with these estimates, the effective molarity[11] calculated from the rate data (k_{cat}/k_{uncat}) gives a value of 2.4 M for the encapsulated reactants.

The results here augur well for the application of reversibly formed molecular assemblies as reaction chambers. If the size and shape selectivity observed in their binding of ground states can be extended to preferential recognition of transition states[12,13] or even high-energy intermediates, then true catalysis via encapsulation could result. To release the product, it may be possible to use the approach devised by Hilvert[14] in antibody catalysis, which takes advantage of a subsequent reaction of the Diels–Alder product that alters its shape and affinity for the binding site and forces turnover. The general problem of product inhibition may be overcome in the future by using dissociative processes, reactions that result in an increased number of encapsulated species. At present, the evidence reported here indicates that in addition to heat, pressure, acids, antibodies[14], micelles[15–18], medium[19,20] and template effects[21], Diels–Alder reactions can also be promoted by reversible encapsulation. □

Received 14 August; accepted 31 October 1996.

1. Sherman, J. C. & Cram, D. J. *J. Am. Chem. Soc.* **117,** 4527–4528 (1989).
2. Garel, L., Dutasta, J.-P. & Collet, A. *Angew. Chem. Int. Edn Engl.* **32,** 1169–1171 (1993).
3. Cram, D. J., Tanner, M. E. & Thomas, R. *Angew. Chem. Int. Edn Engl.* **30,** 1024–1027 (1991).
4. Timmerman, P., Verboom, W., van Veggel, F. C. J. M., van Duynhoven J. P. M. & Reinhoudt, D. N. *Angew. Chem. Int. Edn Engl.* **33,** 2345–2348 (1994).
5. Wyler, R., de Mendoza, J. & Rebek, J. Jr *Angew. Chem. Int. Edn Engl.* **32,** 1699–1701 (1993).
6. Valdés, C., Spitz, U. P., Toledo, L., Kubik, S. & Rebek, J. Jr *J. Am. Chem. Soc.* **117,** 12733–12745 (1995).
7. Meissner, R. S., de Mendoza, J. & Rebek, J. Jr *Science* **270,** 1485–1488 (1995).
8. Kang, J. & Rebek, J. Jr *Nature* **382,** 239–241 (1996).
9. Kelly, T. R., Meghani, P. & Ekkundi, V. S. *Tetrahed. Lett.* **31,** 3381–3384 (1990).
10. Meissner, R., Garcias, X., Mecozzi, S. & Rebek, J. Jr *J. Am. Chem. Soc.* (in the press).
11. Kirby, A. J. *Adv. Phys. Org. Chem.* **17,** 183–278 (1980).
12. Mock, W. L., Irra, T. A., Wepsiec, J. P. & Adhya, M. *J. Org. Chem.* **54,** 5302–5308 (1989).
13. McCurdy, A., Jimenez, L., Stauffer, D. A. & Dougherty, D. A. *J. Am. Chem. Soc.* **114,** 10314–10321 (1992).
14. Hilvert, D., Hill, K. W. & Auditor, M. T. M. *J. Am. Chem. Soc.* **111,** 9261–9263 (1989).
15. Grieco, P. A., Garner, P. & He, Z.-M. *Tetrahedr. Lett.* **24,** 1897–1900 (1983).
16. Breslow, R., Maitra, U. & Rideout, D. *Tetrahedr. Lett.* **24,** 1901–1904 (1983).
17. Braun, R., Schuster, F. & Sauer, J. *Tetrahedr. Lett.* **27,** 1285–1288 (1986).
18. Singh, V. K., Raju, B. N. S. & Deota, P. T. *Synth. Commun.* **18,** 567–574 (1988).
19. Grieco, P. A., Kaufman, M. D., Daeuble, J. F. & Saito, N. *J. Am. Chem. Soc.* **118,** 2095–2096 (1996).
20. Breslow, R. & Guo, T. *J. Am. Chem. Soc.* **110,** 5613–5617 (1988).
21. Walter, C. J., Anderson, H. L. & Sanders, J. K. M. *J. Chem. Soc. Chem. Commun.* 459–460 (1993).
22. Mohamadi, F. *et al. J. Comput. Chem.* **11,** 440–467 (1990).

ACKNOWLEDGEMENTS. We thank J. Brauman, D. Hilvert, J. Stubbe, J. Williamson and M. Heagy for discussions. This work was supported by the National Institutes of Health.

CORRESPONDENCE should be addressed to J.R. at the Skaggs Institute for Chemical Biology (e-mail: jrebek@scripps.edu).

Infrared remote sensing of breaking waves

A. T. Jessup*, C. J. Zappa*, M. R. Loewen† & V. Hesany*

* Applied Physics Laboratory, University of Washington, Seattle, Washington 98195, USA
† Department of Mechanical and Industrial Engineering, University of Toronto, Toronto, Ontario, M5S 3G8, Canada

ENERGY dissipation due to deep-water wave breaking plays a critical role in the development and evolution of the ocean surface wave field. Furthermore, the energy lost by the wave field via the breaking process is a source for turbulent mixing and air entrainment, which enhance air–sea heat and gas transfer[1–3]. But the current lack of reliable methods for measuring energy dissipation associated with wave breaking inhibits the quantitative study of processes occurring at ocean surfaces, and represents a major impediment to the improvement of global wave-prediction models[4]. Here we present a method for remotely quantifying wave-breaking dynamics which uses an infrared imager to measure the temperature changes associated with the disruption and recovery of the surface thermal boundary layer (skin layer). Although our present results focus on quantifying energy dissipation—in particular, we show that the recovery rate of the skin layer in the wakes of breaking waves is correlated with the energy dissipation rate—future applications of this technique should help to elucidate the nature of important small-scale surface processes contributing to air–sea heat[5] and gas[6] flux, and lead to a fuller understanding of general ocean–atmosphere interactions.

Under most circumstances, a net upward heat flux from the ocean to the atmosphere occurs by molecular conduction through the skin layer at the ocean surface. As a result, the surface, or skin, temperature of the ocean is less than the bulk temperature immediately below by a few tenths of a degree Celsius[7,8]. An infrared radiometer measures only the skin temperature because the optical depth of the infrared radiation detected, about 10 μm, is much less than the thickness of the skin layer, of the order of 1 mm (refs 9–11). Our measurements confirm an early result[12] showing that when the cool skin layer is momentarily disrupted by a breaking wave, the skin temperature of the resulting turbulent wake is approximately equal to the bulk temperature. As the wake subsides, the skin layer recovers, and the skin temperature returns to its original, cooler value. Infrared measurements of breaking waves made in the surf zone[12] show a recovery time of the order of 10 s. We have found that the time needed for the skin layer to recover depends on the ambient heat flux[13] and, most significantly for quantifying wave breaking, on the strength of the event. Therefore, infrared measurements of the skin-layer recovery process should provide the capability to remotely monitor free-surface turbulence under conditions of constant heat flux or when the heat flux dependence is known.

Our measurements were made using an infrared imager which provides a time series of two-dimensional images of the skin temperature as inferred from the infrared radiance. Figure 1 shows a sequence of simultaneous video and infrared images of a breaking wave that was taken in the open ocean (time increases *a* to *d*). The first three video images show the breaking wave propagating from right to left as it evolves from a narrow, curved ridge to an actively breaking crest, or whitecap. The first three infrared images show features of increased temperature that clearly correspond to the whitecap, which can be up to 0.1 °C warmer than its wake. Part of the whitecap signature is probably an apparent temperature increase due to increased emissivity[14] associated with surface roughness and bubbles. Of primary interest here is the portion of the wake where the temperature changes are associated with the skin-layer disruption due to breaking-